PAPER

Plasmonic properties of composition graded spherical nanoparticles in quasi-static approximation

To cite this article: Andrei Galiautdinov and Yiping Zhao 2023 *J. Phys. D: Appl. Phys.* **56** 055102

IOP Publishing Journal of Physics D: Applied Physics
J. Phys. D: Appl. Phys. **56** (2023) 055102 (13pp) https://doi.org/10.1088/1361-6463/acad8a

Plasmonic properties of composition graded spherical nanoparticles in quasi-static approximation

Andrei Galiautdinov and Yiping Zhao*

Department of Physics and Astronomy, University of Georgia, Athens, GA 30602, United States of America

E-mail: zhaoy@uga.edu

Received 4 October 2022, revised 14 December 2022
Accepted for publication 21 December 2022
Published 5 January 2023

Abstract

During the operation of a localized surface plasmon resonance (LSPR) sensor made in the form of a core–shell nanoparticle with the shell acting as a sensing layer, the target molecules penetrate into the shell due to intrinsic diffusion or reaction mechanisms. As a result, these molecules or various reactants are nonuniformly distributed in the shell layer. Such sensing particles are termed composition graded plasmonic particles, and their LSPR characteristics may be quite different from those of the uniform core–shell particles. Here, under the quasi-static assumption, a perturbation theory is developed to predict the LSPR properties of composition graded plasmonic particles. The effects of the composition gradient on the LSPR properties due to a metal hydride, a dielectric, and an effective medium are either numerically calculated or analytically derived. Our results show that various configurations of the composition gradient can tune the location and the amplitude of the LSPR peak. The results are important for understanding the sensing performance of composition graded plasmonic particles, and the perturbative treatment presented here can also be used for other composition graded structures.

Keywords: localized surface plasmon resonance, quasi-static approximation, perturbation theory, composition graded plasmonic particles

(Some figures may appear in colour only in the online journal)

1. Introduction

The plasmonic properties of metallic nanoparticles (NPs) have been extensively used in designing new optical devices, chemical and biological sensors, photocatalysts, disease treatment, etc [1, 7, 10–12, 15, 18, 22]. Various types of NPs, such as solid spheres, spherical shells, core–shell spheres, nanorods, cylinders, rings, triangles, etc have been systematically investigated both theoretically and experimentally [5–7, 12, 20]. However, recently another kind of NPs, called composition graded plasmonic NPs, has emerged and demonstrated to have some unique optical properties. For example, Larsen and Zhao fabricated multilayered composition graded Ag–Cu nanotriangle arrays using nanosphere lithography and co-deposition and found that the localized surface plasmon resonance (LSPR) sensitivity could be improved by a factor of two compared to pure Ag nanotriangle arrays of the same size and thickness [8]. In addition, for some LSPR chemical sensing applications, the resulting plasmonic structures are intrinsically composition graded structures. For example, for plasmonic hydrogen sensors (PHSs), either metal or metal alloy plasmonic structures have been used and changes in their plasmonic optical properties during hydrogenation have been investigated [1, 4, 23]. According to the hydrogenation kinetics, for a metal NP, the hydrogenation process experiences four stages [1, 16, 25]: (a) hydrogen adsorption, in which hydrogen is physiosorbed on the metal surface before diffusing into the metal; (b) hydrogen nucleation, in which hydrogen begins to react with the metal to form metal hydride at the appropriate temperature

* Author to whom any correspondence should be addressed.

and pressure, with random hydride patches being formed on the metal surface; (c) hydrogen coalescence, when the hydride patches coalesce and form a hydride shell around a metal NP; (d) hydride shell thickening, in which subsequent metal-hydrogen reactions take place increasing the hydride shell thickness. Thus, during the sensing procedure, the sensing layer becomes a composition graded structure, which motivates a more systematic investigation into the optical and plasmonic properties of the composition graded NPs. In this paper, under the quasi-static assumption, a perturbation theory is developed to predict the LSPR properties of composition graded plasmonic NPs. The perturbation solution for the polarizability is convergent to the exact solution when higher order perturbation terms are included. The results show that the detailed configurations of composition gradient can tune the location and the amplitude of the LSPR peak.

2. Quasistatic perturbation theory for a core-gradient-shell NP

Let us consider a 'core-gradient-shell' (CGS) NP as shown in figure 1. The particle has a uniform core (Region 1) of radius a_c and position-independent dielectric function ε_c, and a shell (Region 2) of outer radius a whose dielectric function $\varepsilon(r)$ varies with a radial distance r. Region 2 represents the composition graded layer, or the active layer for sensing. The entire particle is immersed in a uniform medium (say air or some liquid, Region 3) with the dielectric constant ε_m. This CGS particle is interacting with a plane electromagnetic wave of wavelength λ propagating along the vertical direction with the incident electric field, $\vec{E}_0$, oscillating along the z-axis, as shown in figure 1. The optical properties of the particle can be determined in the quasi-static approximation by assuming $a \ll \lambda$ and finding the electric potential $\phi(r,\theta)$ in the core, the shell, and the outside medium [7, 12]. In the quasi-static approximation, the potential in Regions 1 and 3 satisfies the Laplace equation,

$$\nabla^2\phi(r,\theta) = 0, \tag{1}$$

with

$$\phi_1(r,\theta) = \sum_{n=0}^{\infty} A_n r^n P_n(\cos\theta), \quad 0 < r < a_c, \tag{2}$$

$$\phi_3(r,\theta) = \sum_{n=0}^{\infty} \left[F_n r^n + G_n r^{-(n+1)}\right] P_n(\cos\theta), \quad a < r < \infty, \tag{3}$$

where $P_n(\cos\theta)$ is the Legendre polynomial of order n, θ is the angle between the z-axis and the vector $\vec{r}$ pointing towards the observation point P, and A_n, F_n, G_n are the coefficients to be determined from the boundary conditions. In Region 2, the potential satisfies the equation,

$$\nabla\cdot[\varepsilon(r)\nabla\phi(r,\theta)] = 0, \tag{4}$$

which, in general, cannot be solved analytically. To obviate this problem, we have developed the perturbation theory which is relevant to and motivated by actual experiment. In the majority of sensing applications, the change in the dielectric permittivity is typically small compared to its initial value. This immediately suggests that the permittivity of the gradient region can be written as

$$\varepsilon(r) = \varepsilon^{(0)} + \delta\varepsilon(r), \quad |\delta\varepsilon(r)| \ll |\varepsilon^{(0)}|, \quad a_c < r < a, \tag{5}$$

where $\varepsilon^{(0)}$ is the *initial* r-independent permittivity, and $\delta\varepsilon(r)$ is the r-dependent *change* of permittivity after sensing. Thus, the potential in equation (4) can be written in the form of a series,

$$\phi(r,\theta) = \phi_{(0)}(r,\theta) + \phi_{(1)}(r,\theta) + \phi_{(2)}(r,\theta) + \ldots, \tag{6}$$

where $\phi_{(1)} \sim \delta\varepsilon$, $\phi_{(2)} \sim \delta\varepsilon^2$, etc. The solution can be further simplified by assuming that it has the 'dipole' form,

$$\phi(r,\theta) = f(r)\cos\theta, \tag{7}$$

where now

$$f(r) = f_{(0)}(r) + f_{(1)}(r) + f_{(2)}(r) + \ldots. \tag{8}$$

The reason for adopting the dipole Ansatz is based on the following argument: the number of boundary conditions in our problem, including the one condition at infinity, is equal to five (see the text around equations (23) and (24)), which fixes the five constants in the harmonic expansion; if by setting the remaining constants to zero we somehow manage to find an acceptable solution then, by the uniqueness theorem of electrostatics, we can be certain that this solution is unique and represents the actual solution to our problem (also see appendix).

Plugging equation (7) in equation (4) we get the following differential equation for $f(r)$,

$$\varepsilon(r)\left[f''(r) + \frac{2}{r}f'(r) - \frac{2}{r^2}f(r)\right] + \varepsilon'(r)f'(r) = 0, \tag{9}$$

where prime $'$ indicates differentiation with respect to r. Combining equations (5), (8) and (9), we find, upon separating different orders, the following sequence of equations,

$$0\text{th}: \quad f''_{(0)} + \frac{2}{r}f'_{(0)} - \frac{2}{r^2}f_{(0)} = 0, \tag{10}$$

$$1\text{st}: \quad f''_{(1)} + \frac{2}{r}f'_{(1)} - \frac{2}{r^2}f_{(1)} = -\frac{\delta\varepsilon'}{\varepsilon_{(0)}}f'_{(0)}, \tag{11}$$

$$2\text{nd}: \quad f''_{(2)} + \frac{2}{r}f'_{(2)} - \frac{2}{r^2}f_{(2)} = \frac{\delta\varepsilon\delta\varepsilon'}{\varepsilon^2_{(0)}}f'_{(0)} - \frac{\delta\varepsilon'}{\varepsilon_{(0)}}f'_{(1)}, \tag{12}$$

$$\ldots$$

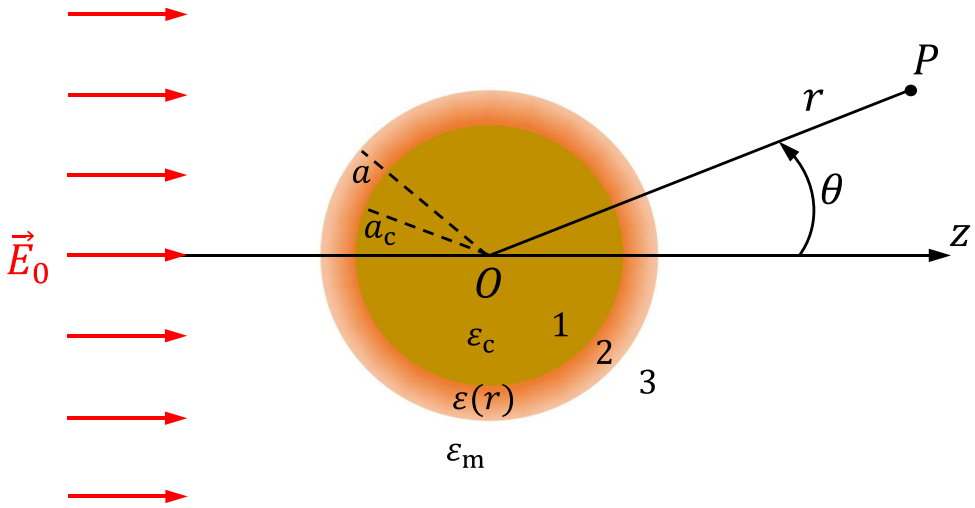

Figure 1. Schematic representation of a core-gradient-shell nanoparticle subjected to the electric field, $\vec{E}_0$ (red arrows), of an incoming electromagnetic wave propagating along the vertical direction. Here, z is the polarization direction, r is the radial distance from particle's center, O, to the point of observation, P, and θ is the corresponding polar angle. In the context of plasmonic hydrogen sensors, the core (Region 1) has radius a_c and is made of plasmonic metal, e.g. silver (Ag), with a fixed and r-independent permittivity, ε_c. The shell (Region 2) has outer radius a and is made of some easily hydrogenated metal, say, palladium (Pd), whose permittivity, $\varepsilon(r)$, changes and becomes r-dependent during the hydrogenation process. When the loading ratio (the number of hydrogen atoms per metal atom in the lattice) is relatively small, shell's permittivity differs from metal's original permittivity by a relatively small amount, which motivates the development of a perturbation theory.

Let us concentrate on the *linear approximation* to $f(r)$, and, correspondingly, to $\phi(r,\theta)$. Here, we only need the general solution to equation (10), which is

$$f_{(0)}(r) = Br + \frac{C}{r^2}, \tag{13}$$

with B and C being some constants, and a particular solution to equation (11), which is

$$f_{(1)}(r) = -y_1(r)\int_{a_c}^{r}\frac{y_2(x)g_{(1)}(x)}{W(y_1(x),y_2(x))}dx + y_2(r)\int_{a_c}^{r}\frac{y_1(x)g_{(1)}(x)}{W(y_1(x),y_2(x))}dx, \tag{14}$$

where $g_{(1)}(r) = -\delta\varepsilon\,'(r)f'_{(0)}(r)/\varepsilon^{(0)}$, and $y_1(r) = r$, $y_2(r) = 1/r^2$ are the fundamental solutions of the homogeneous equation, $f''_{(1)} + (2/r)f'_{(1)} - (2/r^2)f_{(1)} = 0$, whose Wronskian is $W(y_1(r),y_2(r)) = -3/r^2$. Then,

$$f_{(1)}(r) = -r\int_{a_c}^{r}\frac{1}{x^2}\left(-\frac{\delta\varepsilon\,'(x)}{\varepsilon^{(0)}}\right)\left(B-\frac{2C}{x^3}\right)\left(-\frac{x^2}{3}\right)dx + \frac{1}{r^2}\int_{a_c}^{r}x\left(-\frac{\delta\varepsilon\,'(x)}{\varepsilon^{(0)}}\right)\left(B-\frac{2C}{x^3}\right)\left(-\frac{x^2}{3}\right)dx, \tag{15}$$

which gives (after integration by parts), in linear order,

$$f(r) \approx f_{(0)}(r) + f_{(1)}(r) = Br(1+b(r)) + \frac{C}{r^2}(1+c(r)), \tag{16}$$

where

$$b(r) = \frac{\delta\varepsilon(a_c)}{3\varepsilon^{(0)}}\left(1-\frac{a_c^3}{r^3}\right) - \frac{1}{\varepsilon^{(0)}r^3}\int_{a_c}^{r}\delta\varepsilon(x)x^2dx,$$
$$c(r) = \frac{2\delta\varepsilon(a_c)}{3\varepsilon^{(0)}}\left(1-\frac{r^3}{a_c^3}\right) + \frac{2r^3}{\varepsilon^{(0)}}\int_{a_c}^{r}\frac{\delta\varepsilon(x)}{x^4}dx. \tag{17}$$

Additionally, the derivative of $f(r)$ is

$$f'(r) = B(1+b(r)+rb'(r)) - \frac{2C}{r^3}\left(1+c(r)-\frac{rc'(r)}{2}\right), \tag{18}$$

where

$$b'(r) = -\frac{1}{\varepsilon^{(0)}r}\left(\delta\varepsilon(r)-\delta\varepsilon(a_c)\frac{a_c^3}{r^3}\right) + \frac{3}{\varepsilon^{(0)}r^4}\int_{a_c}^{r}\delta\varepsilon(x)x^2dx,$$
$$c'(r) = \frac{2}{\varepsilon^{(0)}r}\left(\delta\varepsilon(r)-\delta\varepsilon(a_c)\frac{r^3}{a_c^3}\right) + \frac{6r^2}{\varepsilon^{(0)}}\int_{a_c}^{r}\frac{\delta\varepsilon(x)}{x^4}dx. \tag{19}$$

Following the discussion in [12] and our perturbative approach, the potentials in the three regions of a CGS NP can be written as

$$\phi_1(r,\theta) = Ar\cos\theta, \quad 0 < r < a_c, \tag{20}$$

$$\phi_2(r,\theta) = \left(Br(1+b(r)) + \frac{C}{r^2}(1+c(r))\right)\cos\theta, \quad a_c < r < a, \tag{21}$$

$$\phi_3(r,\theta) = \left(Fr + \frac{G}{r^2}\right)\cos\theta, \quad a < r < \infty, \tag{22}$$

where $b(r)$, $c(r)$, $b'(r)$, and $c'(r)$ are given in equations (17) and (19). The boundary condition at infinity gives $F = -E_0$, and at $r = a_c$ and $r = a$ the boundary conditions are

$$\begin{aligned} \frac{\partial\phi_1(a_c,\theta)}{\partial\theta} - \frac{\partial\phi_2(a_c,\theta)}{\partial\theta} &= 0, \\ \varepsilon_c\frac{\partial\phi_1(a_c,\theta)}{\partial r} - \varepsilon(a_c)\frac{\partial\phi_2(a_c,\theta)}{\partial r} &= 0, \end{aligned} \tag{23}$$

$$\begin{aligned} \frac{\partial\phi_2(a,\theta)}{\partial\theta} - \frac{\partial\phi_3(a,\theta)}{\partial\theta} &= 0, \\ \varepsilon(a)\frac{\partial\phi_2(a,\theta)}{\partial r} - \varepsilon_m\frac{\partial\phi_3(a,\theta)}{\partial r} &= 0. \end{aligned} \tag{24}$$

In addition,

$$b(a_c) = 0, \quad c(a_c) = 0, \quad b'(a_c) = 0, \quad c'(a_c) = 0, \tag{25}$$

and

$$\begin{aligned} b(a) &= \frac{\delta\varepsilon(a_c)}{3\varepsilon^{(0)}}\left(1 - \frac{a_c^3}{a^3}\right) - \frac{\mathcal{I}_1^{(1)}}{\varepsilon^{(0)}a^3}, \\ c(a) &= \frac{2\delta\varepsilon(a_c)}{3\varepsilon^{(0)}}\left(1 - \frac{a^3}{a_c^3}\right) + \frac{2a^3\mathcal{I}_2^{(1)}}{\varepsilon^{(0)}}, \end{aligned} \tag{26}$$

$$\begin{aligned} b'(a) &= -\frac{1}{\varepsilon^{(0)}a}\left(\delta\varepsilon(a) - \delta\varepsilon(a_c)\frac{a_c^3}{a^3}\right) + \frac{3\mathcal{I}_1^{(1)}}{\varepsilon^{(0)}a^4}, \\ c'(a) &= \frac{2}{\varepsilon^{(0)}a}\left(\delta\varepsilon(a) - \delta\varepsilon(a_c)\frac{a^3}{a_c^3}\right) + \frac{6a^2\mathcal{I}_2^{(1)}}{\varepsilon^{(0)}}, \end{aligned} \tag{27}$$

where we introduced the two integrals,

$$\mathcal{I}_1^{(1)} \equiv \int_{a_c}^{a}\delta\varepsilon(r)\,r^2dr, \quad \mathcal{I}_2^{(1)} \equiv \int_{a_c}^{a}\frac{\delta\varepsilon(r)}{r^4}dr. \tag{28}$$

Retaining the terms up to linear order in $\delta\varepsilon$, the four boundary conditions lead to the following expressions for the coefficients,

$$\begin{aligned} A/E_0 = &-\frac{9\varepsilon^{(0)}\varepsilon_m}{\left(\varepsilon_c + 2\varepsilon^{(0)}\right)\left(\varepsilon^{(0)} + 2\varepsilon_m\right) + 2f_c\left(\varepsilon_c - \varepsilon^{(0)}\right)\left(\varepsilon^{(0)} - \varepsilon_m\right)} \\ &+ \frac{18\varepsilon_m\left(\left(\mathcal{I}_1^{(1)}/a^3\right)\left(\varepsilon_c + 2\varepsilon^{(0)}\right)\left(\varepsilon^{(0)} - \varepsilon_m\right) - a_c^3\mathcal{I}_2^{(1)}\left(\varepsilon_c - \varepsilon^{(0)}\right)\left(\varepsilon^{(0)} + 2\varepsilon_m\right)\right)}{\left(\left(\varepsilon_c + 2\varepsilon^{(0)}\right)\left(\varepsilon^{(0)} + 2\varepsilon_m\right) + 2f_c\left(\varepsilon_c - \varepsilon^{(0)}\right)\left(\varepsilon^{(0)} - \varepsilon_m\right)\right)^2}, \end{aligned} \tag{29}$$

$$\begin{aligned} B/E_0 = &-\frac{3\left(\varepsilon_c + 2\varepsilon^{(0)}\right)\varepsilon_m}{\left(\varepsilon_c + 2\varepsilon^{(0)}\right)\left(\varepsilon^{(0)} + 2\varepsilon_m\right) + 2f_c\left(\varepsilon_c - \varepsilon^{(0)}\right)\left(\varepsilon^{(0)} - \varepsilon_m\right)} \\ &+ \frac{3\varepsilon_m\left(\varepsilon_c + 2\varepsilon^{(0)}\right)\left(\varepsilon_c\delta\varepsilon(a_c)\left(\varepsilon^{(0)} + 2\varepsilon_m\right) + 2(\mathcal{I}_1^{(1)}/a^3)\left(\varepsilon_c + 2\varepsilon^{(0)}\right)\left(\varepsilon^{(0)} - \varepsilon_m\right)\right)}{\varepsilon^{(0)}\left(\left(\varepsilon_c + 2\varepsilon^{(0)}\right)\left(\varepsilon^{(0)} + 2\varepsilon_m\right) + 2f_c\left(\varepsilon_c - \varepsilon^{(0)}\right)\left(\varepsilon^{(0)} - \varepsilon_m\right)\right)^2} \\ &+ \frac{6\varepsilon_m f_c\left(\varepsilon_c - \varepsilon^{(0)}\right)\left(\varepsilon_c\delta\varepsilon(a_c)\left(\varepsilon^{(0)} - \varepsilon_m\right) - a^3\mathcal{I}_2^{(1)}\left(\varepsilon_c + 2\varepsilon^{(0)}\right)\left(\varepsilon^{(0)} + 2\varepsilon_m\right)\right)}{\varepsilon^{(0)}\left(\left(\varepsilon_c + 2\varepsilon^{(0)}\right)\left(\varepsilon^{(0)} + 2\varepsilon_m\right) + 2f_c\left(\varepsilon_c - \varepsilon^{(0)}\right)\left(\varepsilon^{(0)} - \varepsilon_m\right)\right)^2}, \end{aligned} \tag{30}$$

$$\begin{aligned} C/E_0 = &\frac{3a_c^3\left(\varepsilon_c - \varepsilon^{(0)}\right)\varepsilon_m}{\left(\varepsilon_c + 2\varepsilon^{(0)}\right)\left(\varepsilon^{(0)} + 2\varepsilon_m\right) + 2f_c\left(\varepsilon_c - \varepsilon^{(0)}\right)\left(\varepsilon^{(0)} - \varepsilon_m\right)} \\ &- \frac{3a_c^3\varepsilon_m\left(\varepsilon_c + 2\varepsilon^{(0)}\right)\left(\varepsilon_c\delta\varepsilon(a_c)\left(\varepsilon^{(0)} + 2\varepsilon_m\right) + 2(\mathcal{I}_1^{(1)}/a^3)(\varepsilon_c - \varepsilon^{(0)})\left(\varepsilon^{(0)} - \varepsilon_m\right)\right)}{\varepsilon^{(0)}\left(\left(\varepsilon_c + 2\varepsilon^{(0)}\right)\left(\varepsilon^{(0)} + 2\varepsilon_m\right) + 2f_c\left(\varepsilon_c - \varepsilon^{(0)}\right)\left(\varepsilon^{(0)} - \varepsilon_m\right)\right)^2} \\ &- \frac{6a_c^3\varepsilon_m f_c\left(\varepsilon_c - \varepsilon^{(0)}\right)\left(\varepsilon_c\delta\varepsilon(a_c)\left(\varepsilon^{(0)} - \varepsilon_m\right) - a^3\mathcal{I}_2^{(1)}(\varepsilon_c - \varepsilon^{(0)})\left(\varepsilon^{(0)} + 2\varepsilon_m\right)\right)}{\varepsilon^{(0)}\left(\left(\varepsilon_c + 2\varepsilon^{(0)}\right)\left(\varepsilon^{(0)} + 2\varepsilon_m\right) + 2f_c\left(\varepsilon_c - \varepsilon^{(0)}\right)\left(\varepsilon^{(0)} - \varepsilon_m\right)\right)^2}, \end{aligned} \tag{31}$$

as well as $G/E_0 = \alpha/(4\pi)$, with the corresponding polarizability (which is our main result), α, being,

$$\begin{aligned}\frac{\alpha}{4\pi a^3} &\approx \frac{\alpha^{(0)}}{4\pi a^3} + \frac{\alpha^{(1)}}{4\pi a^3} \\ &= \frac{\left(\varepsilon_c + 2\varepsilon^{(0)}\right)\left(\varepsilon^{(0)} - \varepsilon_m\right) + f_c\left(\varepsilon_c - \varepsilon^{(0)}\right)\left(2\varepsilon^{(0)} + \varepsilon_m\right)}{\left(\varepsilon_c + 2\varepsilon^{(0)}\right)\left(\varepsilon^{(0)} + 2\varepsilon_m\right) + 2f_c\left(\varepsilon_c - \varepsilon^{(0)}\right)\left(\varepsilon^{(0)} - \varepsilon_m\right)} \\ &\quad + \frac{9\varepsilon_m\left(\left(\mathcal{I}_1^{(1)}/a^3\right)\left(\varepsilon_c + 2\varepsilon^{(0)}\right)^2 + 2\left(a_c^3\mathcal{I}_2^{(1)}\right)f_c\left(\varepsilon_c - \varepsilon^{(0)}\right)^2\right)}{\left(\left(\varepsilon_c + 2\varepsilon^{(0)}\right)\left(\varepsilon^{(0)} + 2\varepsilon_m\right) + 2f_c\left(\varepsilon_c - \varepsilon^{(0)}\right)\left(\varepsilon^{(0)} - \varepsilon_m\right)\right)^2},\end{aligned} \tag{32}$$

where $f_c \equiv a_c^3/a^3$ is the core-to-particle volume ratio, and $\mathcal{I}_1^{(1)}$, $\mathcal{I}_2^{(1)}$ are given in equation (28). Notice that the first term in equation (32) is the usual expression for unperturbed core–shell NP [2] (also see appendix, equation (A17)) and the second term is the linear correction due to the perturbation of shell's permittivity. The second order correction can also be worked out using the general theory, though the calculation is quite lengthy. The final result is

$$\begin{aligned}\frac{\alpha^{(2)}}{4\pi a^3} &= \frac{-3\varepsilon_m}{\varepsilon^{(0)}\left(\left(\varepsilon_c + 2\varepsilon^{(0)}\right)\left(\varepsilon^{(0)} + 2\varepsilon_m\right) + 2f_c\left(\varepsilon_c - \varepsilon^{(0)}\right)\left(\varepsilon^{(0)} - \varepsilon_m\right)\right)^3} \\ &\quad \times \Bigg\{ 6\left(\mathcal{I}_1^{(1)}/a^3\right)^2\left(\varepsilon_c + 2\varepsilon^{(0)}\right)^3\left(\varepsilon^{(0)} - \varepsilon_m\right) \\ &\quad - 12f_c\left(a_c^3\mathcal{I}_2^{(1)}\right)^2\left(\varepsilon_c - \varepsilon^{(0)}\right)^3\left(\varepsilon^{(0)} + 2\varepsilon_m\right) \\ &\quad - 6f_c\mathcal{I}_1^{(1)}\mathcal{I}_2^{(1)}\left(\varepsilon_c - \varepsilon^{(0)}\right)\left(\varepsilon_c + 2\varepsilon^{(0)}\right) \\ &\quad \times \Big(\left(\varepsilon_c + 2\varepsilon^{(0)}\right)\left(\varepsilon^{(0)} + 2\varepsilon_m\right) - 2f_c\left(\varepsilon_c - \varepsilon^{(0)}\right) \\ &\quad \times \left(\varepsilon^{(0)} - \varepsilon_m\right)\Big) + \Big(\left(\varepsilon_c + 2\varepsilon^{(0)}\right)\left(\varepsilon^{(0)} + 2\varepsilon_m\right) \\ &\quad + 2f_c\left(\varepsilon_c - \varepsilon^{(0)}\right)\left(\varepsilon^{(0)} - \varepsilon_m\right)\Big) \\ &\quad \times \Big[\left(\mathcal{J}_1^{(2)}/a^3\right)\left(\varepsilon_c + 2\varepsilon^{(0)}\right)^2 + 4f_c\left(a_c^3\mathcal{J}_2^{(2)}\right)\left(\varepsilon_c - \varepsilon^{(0)}\right)^2 \\ &\quad + 2f_c\left(2\mathcal{J}_3^{(2)} + 3\mathcal{J}_4^{(2)} - 3\mathcal{J}_5^{(2)}\right)\left(\varepsilon_c - \varepsilon^{(0)}\right) \\ &\quad \times \left(\varepsilon_c + 2\varepsilon^{(0)}\right)\Big]\Bigg\},\end{aligned} \tag{33}$$

where $\mathcal{I}_1^{(1)}$, $\mathcal{I}_2^{(1)}$ are again given in equation (28), and

$$\begin{aligned}\mathcal{J}_1^{(2)} &= \int_{a_c}^{a}(\delta\varepsilon(r))^2 r^2 dr, \quad \mathcal{J}_2^{(2)} = \int_{a_c}^{a}\frac{(\delta\varepsilon(r))^2}{r^4}dr, \\ \mathcal{J}_3^{(2)} &= \int_{a_c}^{a}\frac{(\delta\varepsilon(r))^2}{r}dr,\end{aligned} \tag{34}$$

$$\begin{aligned}\mathcal{J}_4^{(2)} &= \int_{a_c}^{a}\delta\varepsilon(r)\,r^2\int_{a_c}^{r}\frac{\delta\varepsilon(s)}{s^4}ds\,dr, \\ \mathcal{J}_5^{(2)} &= \int_{a_c}^{a}\frac{\delta\varepsilon(r)}{r^4}\int_{a_c}^{r}\delta\varepsilon(s)\,s^2 ds\,dr.\end{aligned} \tag{35}$$

3. Core–shell NP with uniformly perturbed shell (no *r*-dependence)

To verify that our expressions for polarizability, equations (32) and (33), make sense, let us consider a very special case with

$$\varepsilon = \varepsilon^{(0)} + \delta\varepsilon, \quad |\delta\varepsilon| \ll |\varepsilon^{(0)}|, \quad \delta\varepsilon = \text{constant}, \tag{36}$$

representing a core–shell NP whose shell, while remaining *uniform*, has permittivity perturbed by a small but constant amount. In that situation,

$$\begin{aligned}&\mathcal{I}_1^{(1)} = \frac{\delta\varepsilon a^3(1-f_c)}{3}, \quad \mathcal{I}_2^{(1)} = \frac{\delta\varepsilon(1-f_c)}{3a_c^3}, \quad \mathcal{J}_1^{(2)} = \delta\varepsilon\mathcal{I}_1^{(1)}, \\ &\mathcal{J}_2^{(2)} = \delta\varepsilon\mathcal{I}_2^{(1)}, \\ &\mathcal{J}_3^{(2)} = (\delta\varepsilon)^2\ln\left(\frac{a}{a_c}\right), \quad \mathcal{J}_4^{(2)} = \frac{(\delta\varepsilon)^2}{9}\left[\frac{1-f_c}{f_c} - 3\ln\left(\frac{a}{a_c}\right)\right], \\ &\mathcal{J}_5^{(2)} = -\frac{(\delta\varepsilon)^2}{9}\left[1 - f_c - 3\ln\left(\frac{a}{a_c}\right)\right],\end{aligned} \tag{37}$$

and the expression for polarizability becomes,

$$\begin{aligned}\frac{\alpha}{4\pi a^3} &\approx \frac{\left(\varepsilon_c + 2\varepsilon^{(0)}\right)\left(\varepsilon^{(0)} - \varepsilon_m\right) + f_c\left(\varepsilon_c - \varepsilon^{(0)}\right)\left(2\varepsilon^{(0)} + \varepsilon_m\right)}{\left(\varepsilon_c + 2\varepsilon^{(0)}\right)\left(\varepsilon^{(0)} + 2\varepsilon_m\right) + 2f_c\left(\varepsilon_c - \varepsilon^{(0)}\right)\left(\varepsilon^{(0)} - \varepsilon_m\right)} + \frac{3\delta\varepsilon\varepsilon_m(1-f_c)\left(\left(\varepsilon_c + 2\varepsilon^{(0)}\right)^2 + 2f_c\left(\varepsilon_c - \varepsilon^{(0)}\right)^2\right)}{\left(\left(\varepsilon_c + 2\varepsilon^{(0)}\right)\left(\varepsilon^{(0)} + 2\varepsilon_m\right) + 2f_c\left(\varepsilon_c - \varepsilon^{(0)}\right)\left(\varepsilon^{(0)} - \varepsilon_m\right)\right)^2} \\ &\quad - \frac{3(\delta\varepsilon)^2\varepsilon_m(1-f_c)\left\{\left(\varepsilon_c + 2\varepsilon^{(0)}\right)^3 - 2f_c\left[2(\varepsilon^{(0)})^2\left(\varepsilon^{(0)} + 6\varepsilon_c\right) - \varepsilon_c^2\left(3\varepsilon^{(0)} + 2\varepsilon_c + 9\varepsilon_m\right)\right] + 4f_c^2(\varepsilon_c - \varepsilon^{(0)})^3\right\}}{\left(\left(\varepsilon_c + 2\varepsilon^{(0)}\right)\left(\varepsilon^{(0)} + 2\varepsilon_m\right) + 2f_c\left(\varepsilon_c - \varepsilon^{(0)}\right)\left(\varepsilon^{(0)} - \varepsilon_m\right)\right)^3},\end{aligned} \tag{38}$$

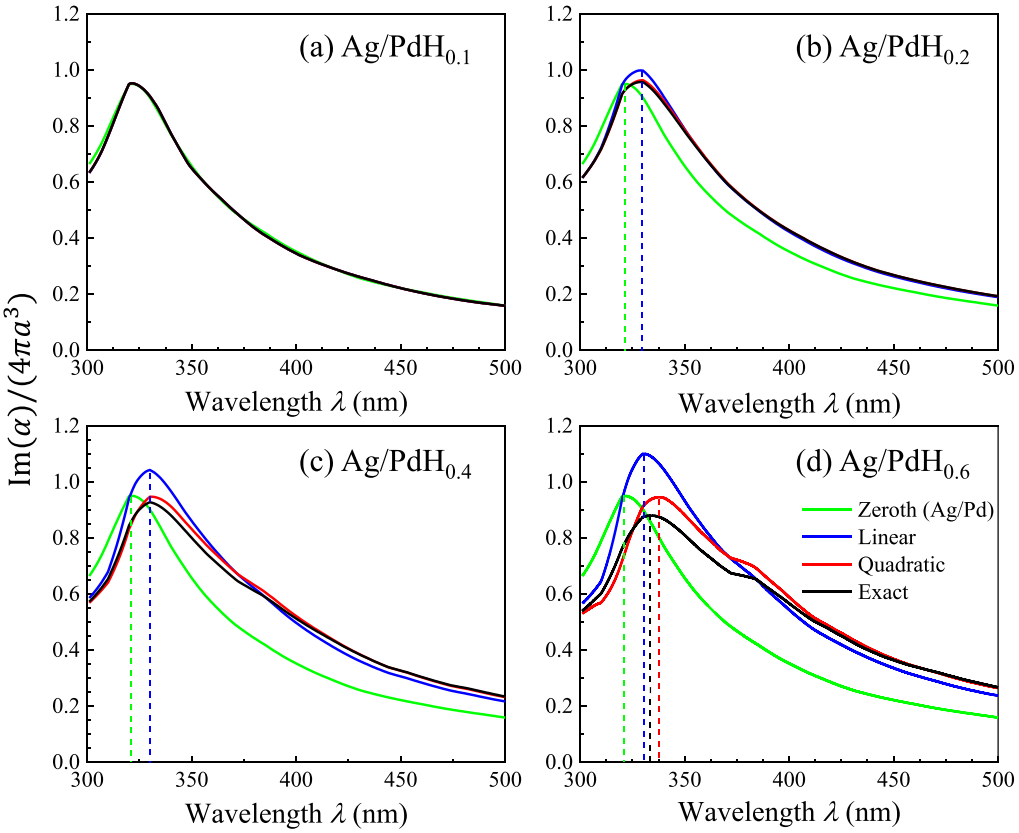

Figure 2. Plots of $\mathrm{Im}(\alpha)/(4\pi a^3)$ in the quasi-static approximation for Ag/PdH$_x$ core–shell NPs based on equation (32) (zeroth order approximation, with $\delta\varepsilon = 0$, green; linear approximation, blue), (38) (quadratic approximation, red), and (39) (exact, black). Here, $f_c = (3/4)^3$, $\varepsilon_m = 1.0006$, and the loading ratios (the number of hydrogen atoms per palladium atom in the lattice) are $x = 0.1$, 0.2, 0.4, and 0.6.

which is identical to the Taylor expansion of the exact formula,

$$\left(\frac{\alpha}{4\pi a^3}\right)_{\text{exact}} = \frac{\left(\varepsilon_c + 2(\varepsilon^{(0)}+\delta\varepsilon)\right)\left((\varepsilon^{(0)}+\delta\varepsilon)-\varepsilon_m\right) + f_c\left(\varepsilon_c - (\varepsilon^{(0)}+\delta\varepsilon)\right)\left(2(\varepsilon^{(0)}+\delta\varepsilon)+\varepsilon_m\right)}{\left(\varepsilon_c + 2(\varepsilon^{(0)}+\delta\varepsilon)\right)\left((\varepsilon^{(0)}+\delta\varepsilon)+2\varepsilon_m\right) + 2f_c\left(\varepsilon_c - (\varepsilon^{(0)}+\delta\varepsilon)\right)\left((\varepsilon^{(0)}+\delta\varepsilon)-\varepsilon_m\right)}, \tag{39}$$

for a core–shell NP given in [2].

To test our approximation scheme, we apply it to a realistic situation involving an Ag/PdH$_x$ core–shell NP with a silver core and a homogeneous shell made of hydrogenated palladium. The goal is to compare the imaginary parts of the core–shell polarizability calculated on the basis of equations (38) and (39), and then decide if the scheme could reliably be applied to more complicated CGS scenarios. The calculations are based on experimental dielectric functions given in [17, 24]. No size effects, other than the effect of the volume ratio f_c on polarizability, are taken into account. The numerical results are presented in figure 2. The results show that, even at relatively large loading ratios (up to about $x = 0.4$), the linear approximation works well to predict the resonant peak's location (see the blue dashed lines in figures 2(b) and (c)), but fails at predicting its amplitude. However, when quadratic correction is also included, the approximate formula does a good job predicting both, which gives us confidence that the second order perturbation theory would also work well in gradient scenarios. For a much higher x (~ 0.6, see figure 2(d)), the linear approximation underestimates while quadratic approximation overestimates the resonant wavelength compared to that given by the exact solution.

4. Core–shell NP with graded (*r*-dependent) shell

The above argument validates correctness of equations (32) and (33). For arbitrary $\delta\varepsilon(r)$ we re-write equation (32) as

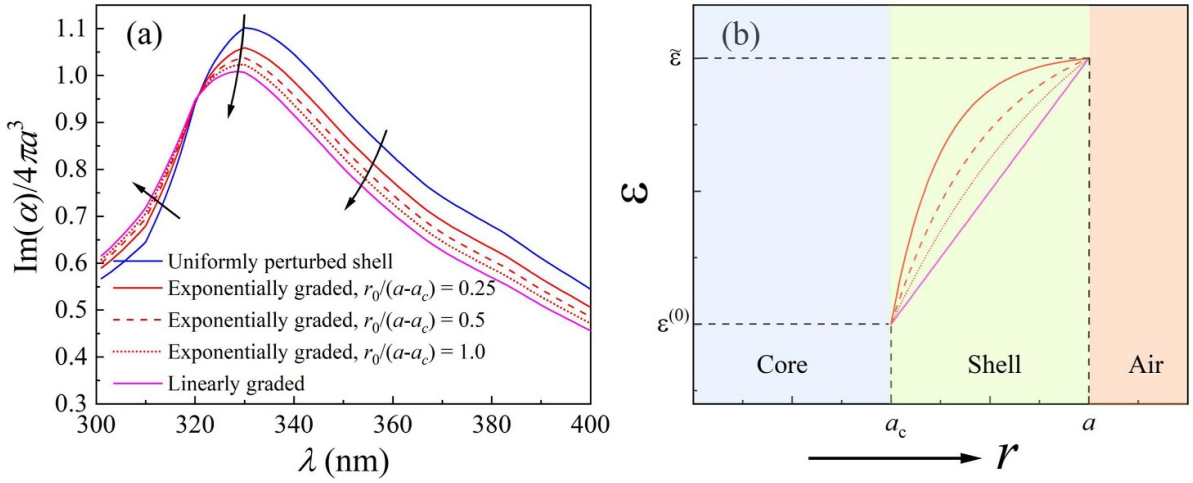

Figure 3. (a) Plots of $\mathrm{Im}(\alpha)/(3V)$ in first-order quasi-static approximation for Ag/PdH_x ($x = 0.6$) core–shell NPs with the linearly and exponentially graded shells calculated based on equations (40), (42) and (43). (b) The composition gradient induced ε distribution in the shell for (a). The line styles are consistent with those in (a).

$$\frac{\alpha}{3V} = \frac{\left(\varepsilon_c + 2\varepsilon^{(0)}\right)\left(\varepsilon^{(0)} - \varepsilon_m\right) + f_c\left(\varepsilon_c - \varepsilon^{(0)}\right)\left(2\varepsilon^{(0)} + \varepsilon_m\right)}{\left(\varepsilon_c + 2\varepsilon^{(0)}\right)\left(\varepsilon^{(0)} + 2\varepsilon_m\right) + 2f_c\left(\varepsilon_c - \varepsilon^{(0)}\right)\left(\varepsilon^{(0)} - \varepsilon_m\right)} + \frac{3\varepsilon_m(1-f_c)\left(\langle\delta\varepsilon\rangle\left(\varepsilon_c + 2\varepsilon^{(0)}\right)^2 + 2f_c\left\langle\frac{a^3a_c^3}{r^6}\delta\varepsilon\right\rangle\left(\varepsilon_c - \varepsilon^{(0)}\right)^2\right)}{\left[\left(\varepsilon_c + 2\varepsilon^{(0)}\right)\left(\varepsilon^{(0)} + 2\varepsilon_m\right) + 2f_c\left(\varepsilon_c - \varepsilon^{(0)}\right)\left(\varepsilon^{(0)} - \varepsilon_m\right)\right]^2}, \tag{40}$$

where $V = (4\pi/3)a^3$, and

$$\langle\delta\varepsilon\rangle \equiv \frac{1}{V_{\mathrm{shell}}}\int_{a_c}^{a}\delta\varepsilon(r)\,4\pi r^2 dr,$$
$$\left\langle\frac{a^3a_c^3}{r^6}\delta\varepsilon\right\rangle \equiv \frac{a^3a_c^3}{V_{\mathrm{shell}}}\int_{a_c}^{a}\frac{\delta\varepsilon(r)}{r^6}\,4\pi r^2 dr, \tag{41}$$

are the two respective averages over the volume of the shell, $V_{\mathrm{shell}} = (4\pi/3)(a^3 - a_c^3)$. Notice that in the uniformly perturbed case both averages give $\delta\varepsilon$, which is just a constant, recovering the first two terms of equation (38).

4.1. Phenomenological model

It is expected that the functional form of $\delta\varepsilon(r)$ may affect CGS particle's polarizability. Therefore, let us consider two simple graded shell scenarios: the linearly graded scenario, with

$$\delta\varepsilon(r) = \varepsilon(r) - \varepsilon^{(0)} = \left(\tilde{\varepsilon} - \varepsilon^{(0)}\right)\frac{r - a_c}{a - a_c}, \tag{42}$$

and the exponentially graded scenario, with

$$\delta\varepsilon(r) = \varepsilon(r) - \varepsilon^{(0)} = \left(\tilde{\varepsilon} - \varepsilon^{(0)}\right)\frac{e^{-(r-a_c)/r_0} - 1}{e^{-(a-a_c)/r_0} - 1}, \tag{43}$$

where, in the context of sensor applications for certain concentrations of targeting analytes, we may take $\varepsilon(r = a_c) = \varepsilon^{(0)}$, $\varepsilon(r = a) = \tilde{\varepsilon}$, and r_0 is the characteristic length of the dielectric distribution.

The analytical results for equation (40) based on either equation (42) or equation (43) are quite complicated and it is difficult to determine which factor dominates the plasmon response. Instead, we can numerically explore the effects of these two gradient scenarios, as depicted in figure 3. We consider a spherical Ag/PdH_x CGS NP with $f_c = (3/4)^3 \approx 0.42$, with Ag as the core and Pd as the shell. During the hydrogen sensing process, hydrogen will first react with the outer surface of the Pd shell and then diffuse into the Pd layer to form a hydride gradient. According to figure 2, when $x = 0.6$, the uniform Ag/$PdH_{0.6}$ core–shell NP causes a significant shift in the plasmon resonant peak. We can take $\tilde{\varepsilon} \equiv \varepsilon_H$ to be the dielectric function of $PdH_{0.6}$, and $\varepsilon^{(0)} \equiv \varepsilon_{Pd}$ to be the dielectric function of Pd. The solid blue curve in figure 3(a) shows the response of a uniform Ag/$PdH_{0.6}$. For the NPs with exponentially graded shells, as shown in figure 3(a) by the red solid, dashed, and dotted curves for $r_0/(a - a_c) = 0.25$, 0.5, and 1.0, respectively, the entire peak is blue-shifted and its amplitude decreases monotonically, which is converging towards the peak for the Ag/Pd core–shell as shown in figure 2(d). The corresponding dielectric function distributions are shown in figure 3(b). When the value of $r_0/(a - a_c)$ increases, the dielectric function $\varepsilon(r)$ approaches more rapidly $\varepsilon^{(0)}$, which means that the effective depth of hydrogenation in the shell becomes smaller, and the dielectric function changes less effectively at the core–shell interface. For the linear gradient shown by the magenta curve in figure 3(a), the peak further shifts to blue since $\varepsilon(r)$ approaches $\varepsilon^{(0)}$ faster compared to the exponential cases. Clearly the results derived from equations (40), (42) and (43) are in good agreement with the corresponding physical pictures.

4.2. Drude model approximation

Another scenario, which has theoretical interest, is a core–shell NP whose core is a metal with its dielectric function described by the Drude model,

$$\varepsilon_c = 1 - \frac{\omega_p^2}{\omega^2 + i\gamma\omega} = 1 - \frac{(\lambda/\lambda_p)^2}{1 + i(\gamma/\omega_p)(\lambda/\lambda_p)}, \tag{44}$$

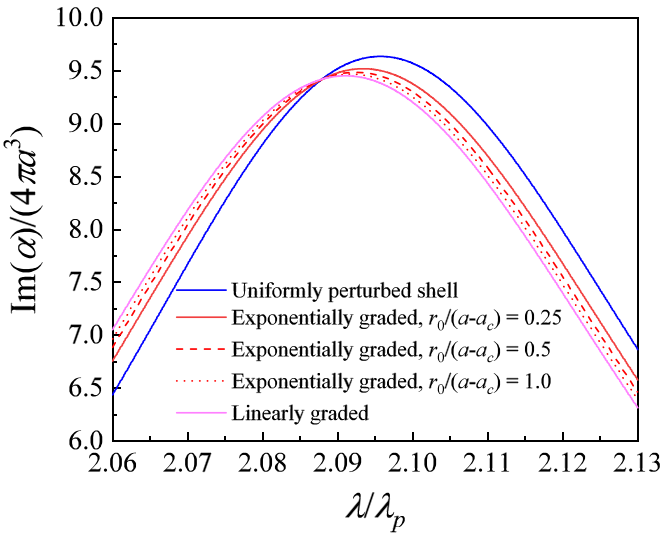

Figure 4. Plots of $\mathrm{Im}(\alpha)/(3V)$ in first-order quasi-static approximation for Drude core-dielectric shells with uniform, linearly, and exponentially graded shells calculated on the basis of equations (40), (42)–(44). Here, $a_c/a = 3/4$, $\gamma/\omega_p = 0.025$, $\varepsilon^{(0)} = 2.5$, $\tilde{\varepsilon} = 2.55$, $\varepsilon_m = 1$.

where ω_p, $\lambda_p = 2\pi c/\omega_p$, and γ are the bulk plasmon frequency, plasmon wavelength, and the damping factor for the metal, with c being the speed of light. The shell is assumed to be made of a dielectric material with real-valued permittivity $\varepsilon(r)$.

If the shell is uniform and $\varepsilon(r) = \varepsilon$ is constant, then, assuming γ/ω_p is small, according to equation (39), the resonant frequency ω_0 is given by

$$\frac{\omega_0}{\omega_p} \approx \sqrt{\frac{z}{z_1}}\left[1 - \frac{1}{8}\frac{z}{z_2}\left(\frac{\gamma}{\omega_p}\right)^2\right], \tag{45}$$

where

$$z = (2\varepsilon+1)(\varepsilon+2\varepsilon_m)^2 - 4f_c^2(\varepsilon-1)(\varepsilon-\varepsilon_m)^2 + 2f_c(\varepsilon+2)(\varepsilon-\varepsilon_m)(\varepsilon+2\varepsilon_m), \tag{46}$$

$$z_1 = \left[(1+2\varepsilon)(\varepsilon+2\varepsilon_m) - 2(\varepsilon-1)(\varepsilon-\varepsilon_m)f_c\right]^2, \tag{47}$$

$$z_2 = \left[\varepsilon(1+2f_c) + 2\varepsilon_m(1-f_c)\right]^2. \tag{48}$$

The polarizabilities of the CGS NPs of a composition graded dielectric shell layer with exponential and linear gradients can be found numerically on the basis on equations (40), (42) and (43), and are plotted in figure 4. In the calculation, we set $a_c/a = 3/4$, $\gamma/\omega_p = 0.025$, $\varepsilon^{(0)} = 2.5$, $\tilde{\varepsilon} = 2.55$, $\varepsilon_m = 1$. Compared to the NP of a metal core with a uniform shell ($\varepsilon = \tilde{\varepsilon} = 2.55$, the solid blue curve in figure 4, with $\lambda_0/\lambda_p = 2.0964$ as predicted on the basis of equation (45)), the polarizabilities of NPs with exponentially graded shells shift to shorter wavelengths (i.e. blue shift, the red curves in figure 4). In addition, the resonant peaks of the red solid, dashed, and dotted curves for $r_0/(a-a_c) = 0.25$, 0.5, and 1.0 shift to shorter λ_0, which is consistent with the observation in figure 3(a). Similarly, the linear gradient (the magenta curve in figure 4) shows the highest blue shift.

4.3. Size effects in the Drude model

It is interesting to investigate the effects of particle's size on the position of the LSPR peak. For that, a full scale numerical simulation of electromagnetic scattering on the NP has to be performed. We found that for our immediate purposes the STRATIFY package developed in [19], which uses recursive transfer-matrix method, is very well suited: it is simple, fast, and reliable. Our simulations, depicted in figure 5, indicate that as the size, a, of the particle decreases the peak shifts towards the predicted quasi-static value, as had to be expected. The quasi-static approximation *underestimates the resonant wavelength*, or, equivalently, *overstimates the resonant frequency*, while in reality ω_{res} should be getting smaller as a increases. In terms of mechanical analogy one may say that this is similar to how the natural frequency of a simple pendulum becomes smaller when its length (size) increases.

4.4. Effective medium approximation for CGS NPs

Equation (40), after simple modification, can also be applied to core–shell NPs with shells made of various *binary* composites. The dielectric function of such composites can often be modeled using the Maxwell-Garnett (MG) effective medium theory in which the host medium and the inclusion are characterized by their respective bulk permittivities, ε_h and ε_i. Denoting the volume fraction of the inclusion by $\eta(r)$ and assuming that $0 \le \eta(r) \ll 1$, the effective permittivity of the composite is given by [3, 13, 14]

$$\varepsilon = \varepsilon_h \frac{1+2\eta\frac{\varepsilon_i-\varepsilon_h}{\varepsilon_i+2\varepsilon_h}}{1-\eta\frac{\varepsilon_i-\varepsilon_h}{\varepsilon_i+2\varepsilon_h}} = \varepsilon_h\left(1+\frac{3\eta(\varepsilon_i-\varepsilon_h)}{\varepsilon_i+2\varepsilon_h-\eta(\varepsilon_i-\varepsilon_h)}\right) = \varepsilon_h\left[1+3\eta\frac{\varepsilon_i-\varepsilon_h}{\varepsilon_i+2\varepsilon_h}+3\eta^2\left(\frac{\varepsilon_i-\varepsilon_h}{\varepsilon_i+2\varepsilon_h}\right)^2+\ldots\right]. \tag{49}$$

In the context of equation (40), in linear order in η, one has

$$\varepsilon = \varepsilon_h(1+3\eta\mathcal{E}_{ih}), \quad \mathcal{E}_{ih} \equiv (\varepsilon_i-\varepsilon_h)/(\varepsilon_i+2\varepsilon_h), \quad \varepsilon^{(0)} = \varepsilon_h, \quad \delta\varepsilon = 3\varepsilon_h\mathcal{E}_{ih}\eta, \tag{50}$$

so that

$$\frac{\alpha}{3V} = \frac{(\varepsilon_c+2\varepsilon_h)(\varepsilon_h-\varepsilon_m)+f_c(\varepsilon_c-\varepsilon_h)(2\varepsilon_h+\varepsilon_m)}{(\varepsilon_c+2\varepsilon_h)(\varepsilon_h+2\varepsilon_m)+2f_c(\varepsilon_c-\varepsilon_h)(\varepsilon_h-\varepsilon_m)} + \frac{9\varepsilon_m\varepsilon_h\mathcal{E}_{ih}(1-f_c)\left(\langle\eta\rangle(\varepsilon_c+2\varepsilon_h)^2+2f_c\left\langle\frac{a^3a_c^3\eta}{r^6}\right\rangle(\varepsilon_c-\varepsilon_h)^2\right)}{\left[(\varepsilon_c+2\varepsilon_h)(\varepsilon_h+2\varepsilon_m)+2f_c(\varepsilon_c-\varepsilon_h)(\varepsilon_h-\varepsilon_m)\right]^2}, \tag{51}$$

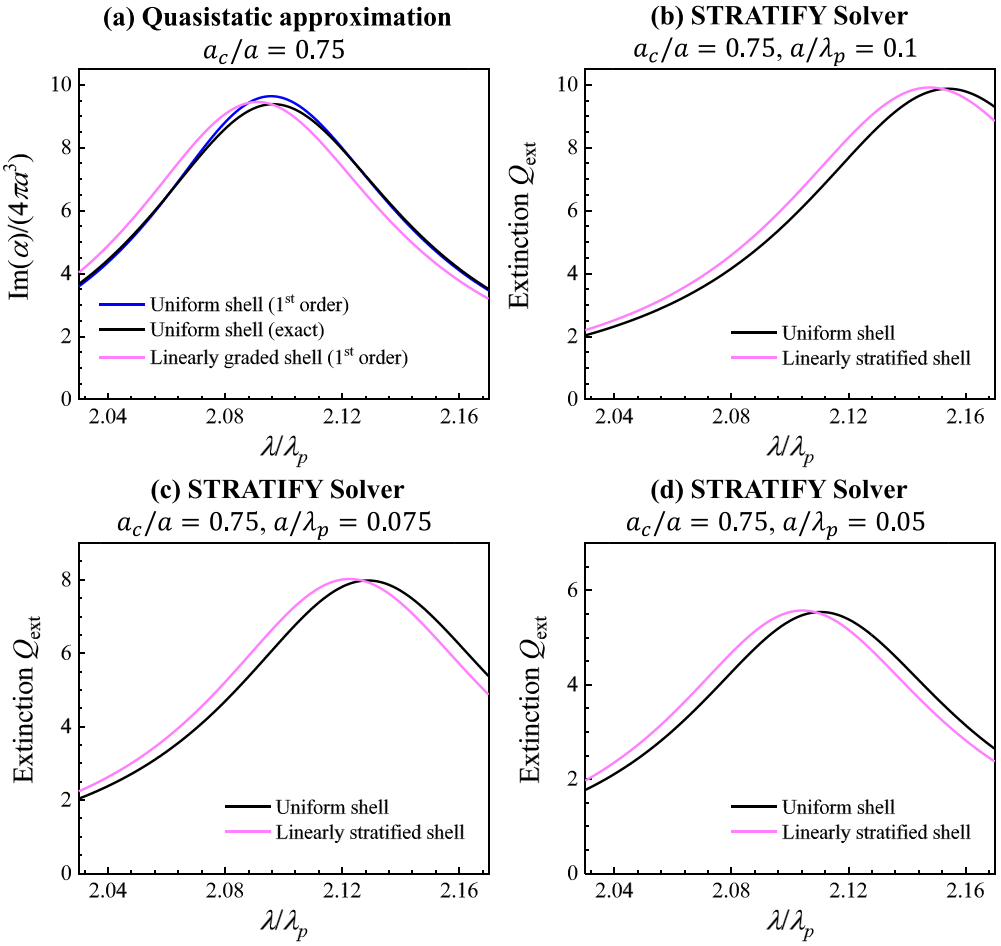

Figure 5. The effect of particle size, a, on the Drude model approximation, equation (44), for a core–shell with same parameters as those used to plot figure 4. Numerical simulations were performed with the help of STRATIFY Maxwell equations solver for MATLAB developed in [19]. For each of the particle sizes, $a/\lambda_{\mathrm{p}} = 0.1, 0.075, 0.05$, the corresponding linearly graded dielectric shell was modeled as a stratified set of ten thin concentric shells with their respective dielectric constants, $\varepsilon_j, j = 1, 2, 3, \ldots, 10$, ranging from $\varepsilon = 2.5$ to 2.55 and varied in accordance with equation (42).

and

$$\langle \eta \rangle \equiv \frac{1}{V_{\mathrm{shell}}} \int_{a_{\mathrm{c}}}^{a} \eta(r) 4\pi r^2 dr,$$
$$\left\langle \frac{a^3 a_{\mathrm{c}}^3 \eta}{r^6} \right\rangle \equiv \frac{a^3 a_{\mathrm{c}}^3}{V_{\mathrm{shell}}} \int_{a_{\mathrm{c}}}^{a} \frac{\eta(r)}{r^6} 4\pi r^2 dr. \tag{52}$$

4.5. Composition-graded NPs and effective medium approximation

If a CGS NP is made *entirely* of a graded material (in which case we call it composition-graded (CG) NP), then the second order approximation can be recovered by taking the limit $a_{\mathrm{c}} \to 0$ in equations (32) and (33), with the final result being,

$$\frac{\alpha}{3V} = \frac{\varepsilon^{(0)} - \varepsilon_{\mathrm{m}}}{\varepsilon^{(0)} + 2\varepsilon_{\mathrm{m}}} + \frac{3\varepsilon_{\mathrm{m}} \langle \delta\varepsilon \rangle}{\left(\varepsilon^{(0)} + 2\varepsilon_{\mathrm{m}}\right)^2} - \frac{\varepsilon_{\mathrm{m}} \left[2\left(\varepsilon^{(0)} - \varepsilon_{\mathrm{m}}\right) \langle \delta\varepsilon \rangle^2 + \left(\varepsilon^{(0)} + 2\varepsilon_{\mathrm{m}}\right) \langle (\delta\varepsilon)^2 \rangle \right]}{\varepsilon^{(0)} \left(\varepsilon^{(0)} + 2\varepsilon_{\mathrm{m}}\right)^3}, \tag{53}$$

where now,

$$\langle \delta\varepsilon \rangle \equiv \frac{1}{V} \int_0^a \delta\varepsilon(r) 4\pi r^2 dr, \quad \langle (\delta\varepsilon)^2 \rangle \equiv \frac{1}{V} \int_0^a (\delta\varepsilon(r))^2 4\pi r^2 dr, \tag{54}$$

are the averages over the entire volume of the sphere, $V = (4\pi/3)a^3$. Then, equation (53) can be used to investigate the plasmonic properties of a CG spherical NP made entirely of a binary composite. We call such particles binary CG spheres. On the basis of the MG theory, equation (49),

$$\varepsilon^{(0)} = \varepsilon_{\mathrm{h}}, \quad \delta\varepsilon \approx 3\varepsilon_{\mathrm{h}} \mathcal{E}_{\mathrm{ih}} \eta + 3\varepsilon_{\mathrm{h}} \mathcal{E}_{\mathrm{ih}}^2 \eta^2,$$
$$(\delta\varepsilon)^2 \approx 9\varepsilon_{\mathrm{h}}^2 \mathcal{E}_{\mathrm{ih}}^2 \eta^2, \quad \mathcal{E}_{\mathrm{ih}} \equiv (\varepsilon_{\mathrm{i}} - \varepsilon_{\mathrm{h}})/(\varepsilon_{\mathrm{i}} + 2\varepsilon_{\mathrm{h}}), \tag{55}$$

where $\eta = \eta(r)$ is the only quantity that is r-dependent. The corresponding averages are,

$$\langle \delta\varepsilon \rangle \approx 3\varepsilon_{\mathrm{h}} \mathcal{E}_{\mathrm{ih}} \langle \eta \rangle + 3\varepsilon_{\mathrm{h}} \mathcal{E}_{\mathrm{ih}}^2 \langle \eta^2 \rangle, \quad \langle \delta\varepsilon \rangle^2 \approx 9\varepsilon_{\mathrm{h}}^2 \mathcal{E}_{\mathrm{ih}}^2 \langle \eta \rangle^2,$$
$$\langle (\delta\varepsilon)^2 \rangle \approx 9\varepsilon_{\mathrm{h}}^2 \mathcal{E}_{\mathrm{ih}}^2 \langle \eta^2 \rangle, \tag{56}$$

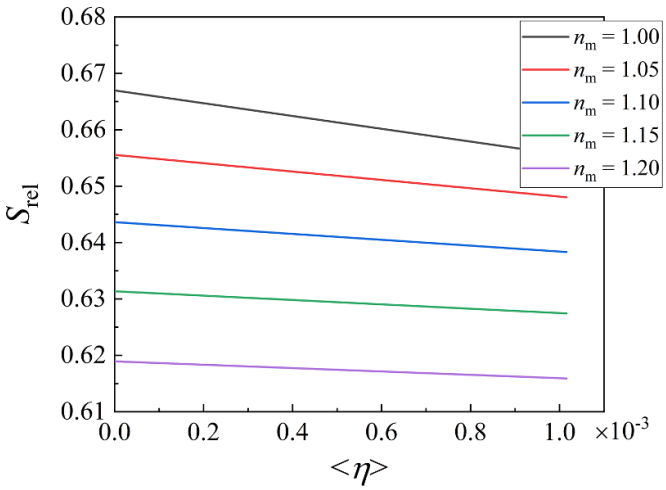

Figure 6. Plot of relative sensitivity, $S_{\rm rel}$, as a function of the averaged inclusion fraction, $\langle\eta\rangle$, for a binary CG spherical NP immersed in environmental media with various indices of refraction, $n_{\rm m}$, equation (63). Here, $\gamma/\omega_{\rm p} = 0.025$, $\varepsilon_{\rm i} = 2.5$.

with

$$\langle\eta\rangle \equiv \frac{1}{V}\int_0^a \eta(r)\,4\pi r^2 dr, \quad \langle\eta^2\rangle \equiv \frac{1}{V}\int_0^a \eta^2(r)\,4\pi r^2 dr. \tag{57}$$

Substituting (55) and (56) into equation (53) gives the expression for the binary CG sphere's polarizability,

$$\frac{\alpha}{3V} = \frac{\varepsilon_{\rm h}-\varepsilon_{\rm m}}{\varepsilon_{\rm h}+2\varepsilon_{\rm m}} + \frac{9\varepsilon_{\rm m}\varepsilon_{\rm h}\mathcal{E}_{\rm ih}\langle\eta\rangle}{(\varepsilon_{\rm h}+2\varepsilon_{\rm m})^2} - \frac{18\varepsilon_{\rm m}\varepsilon_{\rm h}(\varepsilon_{\rm h}-\varepsilon_{\rm m})\mathcal{E}_{\rm ih}^2\langle\eta\rangle^2}{(\varepsilon_{\rm h}+2\varepsilon_{\rm m})^3}, \tag{58}$$

where the terms proportional to $\langle\eta^2\rangle$ canceled out.

Let us take a closer look at the polarizability in equation (58) as a function of the averaged $\langle\eta\rangle$. In the context of optical plasmonic sensors, one possible type of binary composite of interest is a metal host with dielectric inclusion [9]. We take the permittivity $\varepsilon_{\rm i}$ of the dielectric inclusion to be frequency-independent over the frequency range relevant to the problem at hand, and use the simple Drude model, equation (44), for the metal host. For $0 < \gamma/\omega_{\rm p} \ll 1$, assuming that $\langle\eta\rangle$ is sufficiently small, $\langle\eta\rangle \simeq (\gamma/\omega_{\rm p})^2 \ll 1$, to guarantee convergence in equation (58) near the resonance, we find, in linear order in $\langle\eta\rangle$, the inclusion-induced shift, $\delta\omega_0$, in the resonant frequency to be

$$\frac{\delta\omega_0}{\omega_{\rm p}} \approx \frac{-3\varepsilon_{\rm m}}{(2\varepsilon_{\rm m}+1)^{3/2}}\frac{2\varepsilon_{\rm m}+\varepsilon_{\rm i}}{4\varepsilon_{\rm m}-\varepsilon_{\rm i}}\langle\eta\rangle, \tag{59}$$

where (compare with equation (45))

$$\frac{\omega_0}{\omega_{\rm p}} = \sqrt{\frac{2-(2\varepsilon_{\rm m}+1)(\gamma/\omega_{\rm p})^2+\sqrt{16-(2\varepsilon_{\rm m}+1)\left(4-(2\varepsilon_{\rm m}+1)(\gamma/\omega_{\rm p})^2\right)(\gamma/\omega_{\rm p})^2}}{12\varepsilon_{\rm m}+6}} \approx \frac{1}{\sqrt{2\varepsilon_{\rm m}+1}}\left[1-\frac{2\varepsilon_{\rm m}+1}{8}\left(\frac{\gamma}{\omega_{\rm p}}\right)^2\right], \tag{60}$$

is the resonant frequency at $\langle\eta\rangle = 0$ (no inclusion, pure metal sphere). Thus,

$$\frac{\omega_{\rm res}}{\omega_p} \approx \frac{1}{\sqrt{2\varepsilon_{\rm m}+1}}\left[1-\frac{2\varepsilon_{\rm m}+1}{8}\left(\frac{\gamma}{\omega_{\rm p}}\right)^2-\frac{3\varepsilon_{\rm m}}{2\varepsilon_{\rm m}+1}\frac{2\varepsilon_{\rm m}+\varepsilon_{\rm i}}{4\varepsilon_{\rm m}-\varepsilon_{\rm i}}\langle\eta\rangle\right]. \tag{61}$$

Converting this expression to resonant wavelength via $\lambda = 2\pi c/\omega$, and introducing the index of refraction of the surrounding medium via $\varepsilon_{\rm m} = n_{\rm m}^2$, we get,

$$\frac{\lambda_{\rm res}}{\lambda_p} \approx \sqrt{2n_{\rm m}^2+1}\left[1+\frac{2n_{\rm m}^2+1}{8}\left(\frac{\gamma}{\omega_{\rm p}}\right)^2+\frac{3n_{\rm m}^2}{2n_{\rm m}^2+1}\frac{2n_{\rm m}^2+\varepsilon_{\rm i}}{4n_{\rm m}^2-\varepsilon_{\rm i}}\langle\eta\rangle\right]. \tag{62}$$

We can then introduce the *relative* sensitivity with respect to the changes in the environmental index of refraction as

$$S_{\rm rel} \equiv \frac{1}{\lambda_{\rm res}}\frac{d\lambda_{\rm res}}{dn_{\rm m}} = \frac{2n_{\rm m}}{2n_{\rm m}^2+1} + \frac{n_{\rm m}}{2}\left(\frac{\gamma}{\omega_{\rm p}}\right)^2 - \frac{6n_{\rm m}\left(\varepsilon_{\rm i}^2+12\varepsilon_{\rm i}n_{\rm m}^4+4\varepsilon_{\rm i}n_{\rm m}^2-8n_{\rm m}^4\right)}{(2n_{\rm m}^2+1)^2(4n_{\rm m}^2-\varepsilon_{\rm i})^2}\langle\eta\rangle, \tag{63}$$

which is a universal function for any Drude host with dielectric inclusion.

Equation (63) shows that $S_{\rm rel}$ is a linear function of $\langle\eta\rangle$. Figure 6 plots the $S_{\rm rel}$ versus $\langle\eta\rangle$ for a binary CG sphere immersed in various media with different $n_{\rm m}$. We see that

$S_{\rm rel}$ decreases with increasing $\langle\eta\rangle$. This prediction contradicts experimental results observed in [9]. We believe that this discrepancy may be due to the frequency dispersion of the dielectric function of the dielectric inclusion which has not been taken into account in our theoretical analysis.

5. Conclusion

In summary, we developed a physically motivated quasi-static perturbation theory and used it to predict polarizabilities and other plasmonic properties of various composition graded NPs. In contrast to the case of a core–shell with a uniform shell, the polarizability of a core–shell with a composition graded shell was found to be strongly dependent on the functional form of the composition gradient. We showed that the amplitude and the location of the LSPR peak can be tuned by controlling the gradient configuration. The proposed theory may aid in our understanding of the changes in plasmonic properties of certain LSPR sensors with similar kinds of composition gradients. It may also provide theoretical guidance for designing various types of plasmonic structures whose plasmonic properties are needed to be fine tuned for the desired applications. In principle, a similar perturbative approach can also be used in the non-quasi-static regime (of, say, a Mie-type theory), however the details of the corresponding mathematical calculations would likely become prohibitively complicated.

Data availability statement

All data that support the findings of this study are included within the article (and any supplementary files).

Acknowledgments

Y P Z was supported by the National Science Foundation under Grant No. ECCS-1808271.

Appendix. Core-double-shell NP with piece-wise-constant permittivity

Here, for the sake of completeness, we provide a straightforward derivation of polarizability in the quasi-static approximation of a core–shell NP with a double-layer shell, as depicted in figure 7. For an alternative approach to this configuration see, e.g. [21].

In this scenario, in each of the four regions, the quasi-static axially-symmetric potential, $\phi(r,\theta)$, satisfies the Laplace equation, equation (1), together with a total of seven boundary conditions: the six conditions at the three interfaces,

$$\begin{aligned}\frac{\partial\phi_k(a_k,\theta)}{\partial\theta}-\frac{\partial\phi_{k+1}(a_k,\theta)}{\partial\theta}&=0,\\ \varepsilon_k\frac{\partial\phi_k(a_k,\theta)}{\partial r}-\varepsilon_{k+1}\frac{\partial\phi_{k+1}(a_k,\theta)}{\partial r}&=0,\quad k=1,2,3,\end{aligned}\tag{A1}$$

plus one condition at spatial infinity,

$$\phi(r,\theta)|_{r\to\infty}=-E_0z=-E_0r\cos\theta=-E_0rP_1(\cos\theta).\tag{A2}$$

This tells us that our solution should depend on seven constants, which motivates the following Ansatz,

$$\phi_1(r,\theta)=ArP_1(\cos\theta),\quad 0<r<a_1,\tag{A3}$$

$$\phi_2(r,\theta)=\left(Br+\frac{C}{r^2}\right)P_1(\cos\theta),\quad a_1<r<a_2,\tag{A4}$$

$$\phi_3(r,\theta)=\left(Kr+\frac{L}{r^2}\right)P_1(\cos\theta),\quad a_2<r<a_3,\tag{A5}$$

$$\phi_4(r,\theta)=\left(Fr+\frac{G}{r^2}\right)P_1(\cos\theta),\quad a_3<r<\infty.\tag{A6}$$

Condition (A2) then immediately gives, $F=-E_0$, while conditions (A1) result in the system of six linear equations for the coefficients A, B, C, K, L, G,

$$Aa_1=Ba_1+\frac{C}{a_1^2},\tag{A7}$$

$$\varepsilon_1A=\varepsilon_2\left(B-\frac{2C}{a_1^3}\right),\tag{A8}$$

$$Ba_2+\frac{C}{a_2^2}=Ka_2+\frac{L}{a_2^2},\tag{A9}$$

$$\varepsilon_2\left(B-\frac{2C}{a_2^3}\right)=\varepsilon_3\left(K-\frac{2L}{a_2^3}\right),\tag{A10}$$

$$Ka_3+\frac{L}{a_3^2}=Fa_3+\frac{G}{a_3^2},\tag{A11}$$

$$\varepsilon_3\left(K-\frac{2L}{a_3^3}\right)=\varepsilon_4\left(F-\frac{2G}{a_3^3}\right).\tag{A12}$$

When written in matrix form,

$$\left[\begin{array}{cccccc|c}a_1^3&-a_1^3&-1&0&0&0&0\\ \varepsilon_1a_1^3&-\varepsilon_2a_1^3&2\varepsilon_2&0&0&0&0\\ 0&a_2^3&1&-a_2^3&-1&0&0\\ 0&\varepsilon_2a_2^3&-2\varepsilon_2&-\varepsilon_3a_2^3&2\varepsilon_3&0&0\\ 0&0&0&a_3^3&1&-1&a_3^3F\\ 0&0&0&\varepsilon_3a_3^3&-2\varepsilon_3&2\varepsilon_4&\varepsilon_4a_3^3F\end{array}\right],\tag{A13}$$

the system can be solved either by hand using Gaussian elimination or with the help of a symbolic algebra package. The final result is,

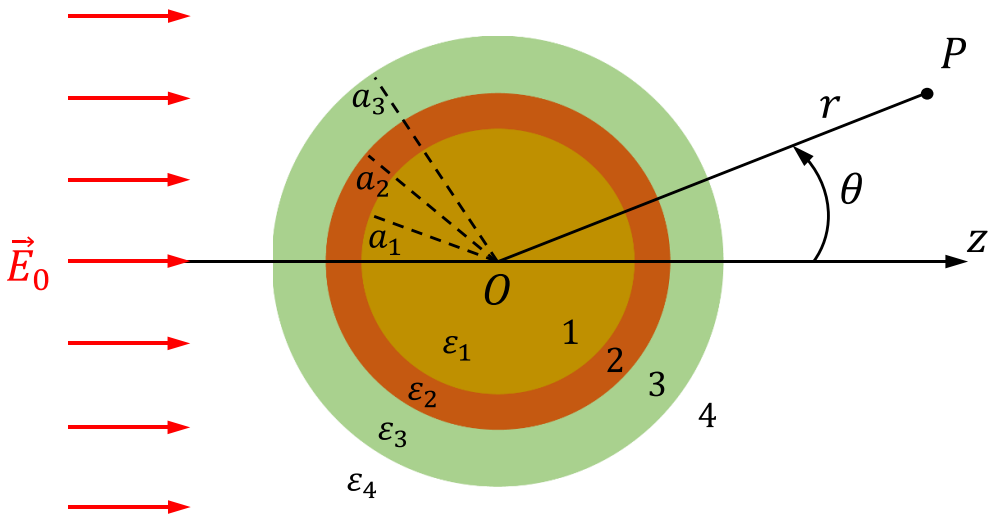

Figure 7. Schematic representation of a core-double-shell nanoparticle subjected to a uniform external field. Here permittivities, $\varepsilon_c \equiv \varepsilon_1$, ε_2, ε_3, $\varepsilon_m \equiv \varepsilon_4$, are assumed to be constant (r-independent).

$$\frac{A}{E_0} = -\frac{27a_2^3a_3^3\varepsilon_2\varepsilon_3\varepsilon_4}{2(\varepsilon_1-\varepsilon_2)\left((2\varepsilon_2+\varepsilon_3)(\varepsilon_3-\varepsilon_4)a_2^3+a_3^3(\varepsilon_2-\varepsilon_3)(\varepsilon_3+2\varepsilon_4)\right)a_1^3+a_2^3(\varepsilon_1+2\varepsilon_2)\left(2(\varepsilon_2-\varepsilon_3)(\varepsilon_3-\varepsilon_4)a_2^3+a_3^3(\varepsilon_2+2\varepsilon_3)(\varepsilon_3+2\varepsilon_4)\right)},$$

$$\frac{B}{E_0} = -\frac{9a_2^3a_3^3(\varepsilon_1+2\varepsilon_2)\varepsilon_3\varepsilon_4}{2(\varepsilon_1-\varepsilon_2)\left((2\varepsilon_2+\varepsilon_3)(\varepsilon_3-\varepsilon_4)a_2^3+a_3^3(\varepsilon_2-\varepsilon_3)(\varepsilon_3+2\varepsilon_4)\right)a_1^3+a_2^3(\varepsilon_1+2\varepsilon_2)\left(2(\varepsilon_2-\varepsilon_3)(\varepsilon_3-\varepsilon_4)a_2^3+a_3^3(\varepsilon_2+2\varepsilon_3)(\varepsilon_3+2\varepsilon_4)\right)},$$

$$\frac{C}{E_0} = \frac{9a_1^3a_2^3a_3^3(\varepsilon_1-\varepsilon_2)\varepsilon_3\varepsilon_4}{2(\varepsilon_1-\varepsilon_2)\left((2\varepsilon_2+\varepsilon_3)(\varepsilon_3-\varepsilon_4)a_2^3+a_3^3(\varepsilon_2-\varepsilon_3)(\varepsilon_3+2\varepsilon_4)\right)a_1^3+a_2^3(\varepsilon_1+2\varepsilon_2)\left(2(\varepsilon_2-\varepsilon_3)(\varepsilon_3-\varepsilon_4)a_2^3+a_3^3(\varepsilon_2+2\varepsilon_3)(\varepsilon_3+2\varepsilon_4)\right)},$$

$$\frac{K}{E_0} = -\frac{3a_3^3\left(2(\varepsilon_1-\varepsilon_2)(\varepsilon_2-\varepsilon_3)a_1^3+a_2^3(\varepsilon_1+2\varepsilon_2)(\varepsilon_2+2\varepsilon_3)\right)\varepsilon_4}{2(\varepsilon_1-\varepsilon_2)\left((2\varepsilon_2+\varepsilon_3)(\varepsilon_3-\varepsilon_4)a_2^3+a_3^3(\varepsilon_2-\varepsilon_3)(\varepsilon_3+2\varepsilon_4)\right)a_1^3+a_2^3(\varepsilon_1+2\varepsilon_2)\left(2(\varepsilon_2-\varepsilon_3)(\varepsilon_3-\varepsilon_4)a_2^3+a_3^3(\varepsilon_2+2\varepsilon_3)(\varepsilon_3+2\varepsilon_4)\right)},$$

$$\frac{L}{E_0} = \frac{3a_2^3a_3^3\left((\varepsilon_1-\varepsilon_2)(2\varepsilon_2+\varepsilon_3)a_1^3+a_2^3(\varepsilon_1+2\varepsilon_2)(\varepsilon_2-\varepsilon_3)\right)\varepsilon_4}{2(\varepsilon_1-\varepsilon_2)\left((2\varepsilon_2+\varepsilon_3)(\varepsilon_3-\varepsilon_4)a_2^3+a_3^3(\varepsilon_2-\varepsilon_3)(\varepsilon_3+2\varepsilon_4)\right)a_1^3+a_2^3(\varepsilon_1+2\varepsilon_2)\left(2(\varepsilon_2-\varepsilon_3)(\varepsilon_3-\varepsilon_4)a_2^3+a_3^3(\varepsilon_2+2\varepsilon_3)(\varepsilon_3+2\varepsilon_4)\right)},$$

$$\frac{G}{E_0} = \frac{a_3^3\left((\varepsilon_1-\varepsilon_2)\left((2\varepsilon_2+\varepsilon_3)(2\varepsilon_3+\varepsilon_4)a_2^3+2a_3^3(\varepsilon_2-\varepsilon_3)(\varepsilon_3-\varepsilon_4)\right)a_1^3+a_2^3(\varepsilon_1+2\varepsilon_2)\left((\varepsilon_2-\varepsilon_3)(2\varepsilon_3+\varepsilon_4)a_2^3+a_3^3(\varepsilon_2+2\varepsilon_3)(\varepsilon_3-\varepsilon_4)\right)\right)}{2(\varepsilon_1-\varepsilon_2)\left((2\varepsilon_2+\varepsilon_3)(\varepsilon_3-\varepsilon_4)a_2^3+a_3^3(\varepsilon_2-\varepsilon_3)(\varepsilon_3+2\varepsilon_4)\right)a_1^3+a_2^3(\varepsilon_1+2\varepsilon_2)\left(2(\varepsilon_2-\varepsilon_3)(\varepsilon_3-\varepsilon_4)a_2^3+a_3^3(\varepsilon_2+2\varepsilon_3)(\varepsilon_3+2\varepsilon_4)\right)}, \tag{A14}$$

with the corresponding polarizability being

$$\frac{\alpha}{4\pi a_3^3} = \frac{(\varepsilon_1+2\varepsilon_2)\left[(\varepsilon_2+2\varepsilon_3)(\varepsilon_3-\varepsilon_4)+f_{23}(\varepsilon_2-\varepsilon_3)(2\varepsilon_3+\varepsilon_4)\right]+f_{12}(\varepsilon_1-\varepsilon_2)\left[2(\varepsilon_2-\varepsilon_3)(\varepsilon_3-\varepsilon_4)+f_{23}(2\varepsilon_2+\varepsilon_3)(2\varepsilon_3+\varepsilon_4)\right]}{(\varepsilon_1+2\varepsilon_2)\left[(\varepsilon_2+2\varepsilon_3)(\varepsilon_3+2\varepsilon_4)+2f_{23}(\varepsilon_2-\varepsilon_3)(\varepsilon_3-\varepsilon_4)\right]+2f_{12}(\varepsilon_1-\varepsilon_2)\left[(\varepsilon_2-\varepsilon_3)(\varepsilon_3+2\varepsilon_4)+f_{23}(2\varepsilon_2+\varepsilon_3)(\varepsilon_3-\varepsilon_4)\right]}, \tag{A15}$$

where we introduced the two volume fractions,

$$f_{12} = a_1^3/a_2^3, \quad f_{23} = a_2^3/a_3^3. \tag{A16}$$

Notice that equation (A15) correctly reproduces the two important cases:

Case 1: Core–shell (with $a_3 = a_2$, $\varepsilon_3 = \varepsilon_2$),

$$\frac{\alpha}{4\pi a_2^3} = \frac{(\varepsilon_1 + 2\varepsilon_2)(\varepsilon_2 - \varepsilon_4) + f_{12}(\varepsilon_1 - \varepsilon_2)(2\varepsilon_2 + \varepsilon_4)}{(\varepsilon_1 + 2\varepsilon_2)(\varepsilon_2 + 2\varepsilon_4) + 2f_{12}(\varepsilon_1 - \varepsilon_2)(\varepsilon_2 - \varepsilon_4)}. \tag{A17}$$

Case 2: Uniform sphere (with $a_3 = a_2 = a_1$, $\varepsilon_3 = \varepsilon_2 = \varepsilon_1$),

$$\frac{\alpha}{4\pi a_1^3} = \frac{\varepsilon_1 - \varepsilon_4}{\varepsilon_1 + 2\varepsilon_4}. \tag{A18}$$

ORCID iDs

Andrei Galiautdinov https://orcid.org/0000-0001-5752-9296
Yiping Zhao https://orcid.org/0000-0002-3710-4159

References

[1] Ai B, Sun Y and Zhao Y 2022 Plasmonic hydrogen sensors *Small* **18** 2107882
[2] Bohren C F and Huffman D R 2008 *Absorption and Scattering of Light by Small Particles* (New York: Wiley)
[3] Choy T C 2015 *Effective Medium Theory: Principles and Applications* vol 165 (Oxford: Oxford University Press)
[4] Darmadi I, Nugroho F A A and Langhammer C 2020 High-performance nanostructured palladium-based hydrogen sensors-current limitations and strategies for their mitigation *ACS Sens.* **5** 3306–27
[5] Downing C A and Weick G 2020 Plasmonic modes in cylindrical nanoparticles and dimers *Proc. R. Soc.* A **476** 20200530
[6] Hohenester U and Trügler A 2012 MNPBEM—a MATLAB toolbox for the simulation of plasmonic nanoparticles *Comput. Phys. Commun.* **183** 370–81
[7] Klimov V 2014 *Nanoplasmonics* (Boca Raton, FL: CRC press)
[8] Larson S, Yang Z and Zhao Y 2019 Improving LSPR sensing performance using multilayered composition graded Ag–Cu nanotriangle arrays *Chem. Commun.* **55** 1342–4
[9] Larson S and Zhao Y 2018 Localized surface plasmonic resonance and sensing properties of Ag–MgF_2 composite nanotriangles *J. Phys. Chem.* C **122** 7374–81
[10] Lee C, Lawrie B, Pooser R, Lee K-G, Rockstuhl C and Tame M 2021 Quantum plasmonic sensors *Chem. Rev.* **121** 4743–804
[11] Luong H M, Pham M T, Guin T, Madhogaria R P, Phan M-H, Larsen G K and Nguyen T D 2021 Sub-second and ppm-level optical sensing of hydrogen using templated control of nano-hydride geometry and composition *Nat. Commun.* **12** 1–10
[12] Maier S A 2007 *Plasmonics: Fundamentals and Applications* vol 1 (Berlin: Springer)
[13] Markel V A 2016 Introduction to the Maxwell Garnett approximation: tutorial *J. Opt. Soc. Am.* A **33** 1244–56
[14] Markel V A 2016 Maxwell Garnett approximation (advanced topics): tutorial *J. Opt. Soc. Am.* A **33** 2237–55
[15] Mayer K M and Hafner J H 2011 Localized surface plasmon resonance sensors *Chem. Rev.* **111** 3828–57
[16] Mintz M H and Zeiri Y 1995 Hydriding kinetics of powders *J. Alloys Compd.* **216** 159–75
[17] Palm K J, Murray J B, Narayan T C and Munday J N 2018 Dynamic optical properties of metal hydrides *ACS Photonics* **5** 4677–86
[18] Petryayeva E and Krull U J 2011 Localized surface plasmon resonance: nanostructures, bioassays and biosensing—a review *Anal. Chim. Acta* **706** 8–24
[19] Rasskazov I L, Scott Carney P and Moroz A 2020 Stratify: a comprehensive and versatile MATLAB code for a multilayered sphere *OSA Contin.* **3** 2290–306
[20] Ruiz M and Schnitzer O 2022 Plasmonic resonances of slender nanometallic rings *Phys. Rev.* B **105** 125412
[21] Selina N V 2019 Metal–dielectric core–shell nanoparticles *Nanotechnol. Russia* **14** 451–5
[22] Stewart M E, Anderton C R, Thompson L B, Maria J, Gray S K, Rogers J A and Nuzzo R G 2008 Nanostructured plasmonic sensors *Chem. Rev.* **108** 494–521
[23] Wadell C, Syrenova S and Langhammer C 2014 Plasmonic hydrogen sensing with nanostructured metal hydrides *ACS Nano* **8** 11925–40
[24] Yang H U, D'Archangel J, Sundheimer M L, Tucker E, Boreman G D and Raschke M B 2015 Optical dielectric function of silver *Phys. Rev.* B **91** 235137
[25] Zhang J Z, Li J, Li Y and Zhao Y 2014 *Hydrogen Generation, Storage and Utilization* (New York: Wiley)